Advanced Fiber Materials
https://doi.org/10.1007/s42765-022-00247-3

RESEARCH ARTICLE

Adaptive Electrospinning System Based on Reinforcement Learning for Uniform-Thickness Nanofiber Air Filters

Seok Hyeon Hwang[1] · Jin Yeong Song[1] · Hyun Il Ryu[1] · Jae Hee Oh[1] · Seungwook Lee[1] · Donggeun Lee[1] · Dong Young Park[2] · Sang Min Park[1]

Received: 13 September 2022 / Accepted: 9 December 2022

Abstract
Electrospinning is a simple and versatile method to produce nanofiber filters. However, owing to bending instability that occurs during the electrospinning process, electrospinning has frequently produced a non-uniform-thickness nanofiber filter, which deteriorates its air filtration. Here, an adaptive electrospinning system based on reinforcement learning (E-RL) was developed to produce uniform-thickness nanofiber filters. The E-RL accomplished a real-time thickness measurement of an electrospun nanofiber filter by measuring the transmitted light through the nanofiber filter using a camera placed at the bottom of the collector and converting it into thickness using the Beer–Lambert law. Based on the measured thickness, the E-RL detected the non-uniformity of the nanofiber filter thickness and manipulated the movable collector to alleviate the non-uniformity of the thickness by a pre-trained reinforcement learning (RL) algorithm. For the training of the RL algorithm, the nanofiber production simulation software based on the empirical model of the deposition of the nanofiber filter was developed, and the training process of the RL algorithm was repeated until the optimal policy was achieved. After the training process with the simulation software, the trained model was transferred to the adaptive electrospinning system. By the movement of the collector under the optimal strategy of RL algorithm, the non-uniformity of such nanofiber filters was significantly reduced by approximately five times in standard deviation and error for both simulation and experiment. This finding has great potential in improving the reliability of electrospinning process and nanofiber filters used in research and industrial fields such as environment, energy, and biomedicine.

Keywords Electrospinning · Nanofiber filter · Uniform thickness · Reinforcement learning · Deep Q-network

Introduction

Electrospinning is a process, used for the facile and effective production of nanofibers and nanofiber filters [1–3]. The configuration of electrospinning consists of a high-voltage supplier, syringe, syringe needle, syringe pump, and metal collector. When a high voltage is applied between the syringe needle and the metal collector with the ejection of polymer solution through the syringe needle, the diameter of the solution jet decreases owing to the evaporation of the solvent and bending instability [2], thereby resulting in nanoscale fibers. During their flight toward the collector, electrospun nanofibers experience chaotic motion and they are deposited into a randomly interwoven nanofiber filter on the collector as shown in Fig. S1.

Electrospun nanofiber filters have been widely used in many laboratories and industrial fields owing to several advantageous properties such as high porosity, large surface-to-volume ratio, low density [4], and large active surface area. For example, nanofiber filters have shown superior performance in air filtration [5, 6], liquid filters, battery separators [7], and tissue membranes [8–12]. Furthermore, many companies have commercialized products using a nanofiber filter, such as electromagnetic interference (EMI) shielding film for protective clothes, skincare packs, automotive filters, HVAC filter, gas turbine filters, and N95/N99 masks.

✉ Sang Min Park
sangmin.park@pusan.ac.kr

[1] School of Mechanical Engineering, Pusan National University, 63-2 Busan University-ro, Geumjeong-gu, Busan 46241, South Korea

[2] Smart Manufacturing Technology R&D Group, Korea Institute of Industrial Technology, 320 Techno Sunhwan-ro, Yuga-eup, Dalseong-gun, Daegu 42994, Republic of Korea

Published online: 09 January 2023

Various properties such as the type of materials, diameter, and density [13, 14] of the nanofibers and the thickness of the nanofiber filter influence the performance of electrospun nanofiber filters [1]. Such nanofiber properties could be controlled by changing electrospinning parameters such as applied voltage, flow rate, solvent, viscosity, solution concentration, temperature, and humidity. However, the deposition control for uniform thickness of the nanofiber filter would not be easily achievable by changing the electrospinning parameters alone, although the thickness of the nanofiber filter plays a significant role in determining the efficiency of the material transport across the nanofiber filter [6, 15]. Current approaches to control the deposition of the nanofiber filter is majorly dependent on a simple and inaccurate technique of changing the electrospinning time, frequently producing a non-uniform-thickness nanofiber filter. Furthermore, bending instability could also lead to the non-uniform deposition of the nanofibers, causing a locally thin region of the nanofiber filter. This thin region of the nanofiber filter would exhibit a low filtration performance or mechanical strength and could induce flow concentration toward the region, thereby causing damage or degradation in the performance of the nanofiber filter. Therefore, developing an electrospinning system that can control the deposition of nanofibers is necessary to achieve uniform deposition.

Recently, the advance in machine learning (ML), a subset of artificial intelligence, facilitates ML-driven systems to resolve engineering challenges such as classification, diagnostics, optimization, and control. Conventional ML can be divided into supervised learning, unsupervised learning, and reinforcement learning (Fig. S2). Supervised learning algorithms such as artificial neural networks (ANN) [16], support vector machines (SVM) [17], k-nearest neighbors [18], decision trees (DTs) [19], and generalized linear model (GLM) [20] have been utilized as predictive models based on input data and labeled output data to solve the regression problems. In addition, convolution neural network (CNN) [21] shows high performance to solve classification problems. Unsupervised learning algorithms such as *K*-means [22], hierarchical cluster analysis (HCA), and t-distributed stochastic neighbor embedding (t-SNE) [23] have been used to cluster data with similarity, pattern, and difference without labeled output data (i.e., with only input data). RL, a subset of ML, is a decision-making algorithm based on behavioral psychology, which interacts with the environment in discrete time steps through trial-and-error methods. RL [24, 25] could effectively determine an optimal control strategy in a random environment that provides uncertain information; thus, RL has been widely utilized in many fields, including energy management [26], robots [27], and automobile control [28], to determine the optimal control strategy.

In this study, an adaptive electrospinning system based on reinforcement learning (E-RL) is proposed for uniform deposition of nanofibers. Considering its effectiveness in finding an optimal control strategy, RL was utilized to achieve uniform deposition by optimally controlling the movable collector. Among various model-free RL algorithms, one of the value function-based approaches, namely double deep *Q*-networks (DDQN) [24], was adopted in the electrospinning system. The DDQN, which showed great performance in playing Atari games [24], was designed to find an optimal control strategy for the movement of a collector to decrease the non-uniformity of the nanofiber filter. In training the DDQN, the thickness of the nanofiber filter was measured in real time and utilized as a state for the DDQN. The thickness of the nanofiber filter was calculated on the basis of the Beer–Lambert law [29] from the light transmittance measured through a CCD camera placed at the bottom of the collector [29], In simplifying the electrospinning system into the 1D problem, a two-parallel-metal-plate collector, which produced a nanofiber filter with the same thickness along the *y*-axis, was adopted. With the incorporation of the DDQN into the electrospinning system, the nanofiber filter with a uniform and desired thickness was achieved by moving the collector based on the optimal control strategy obtained from the DDQN. Finally, the improved uniformity and performance of air filtration of the nanofiber mat fabricated by E-RL were demonstrated, and such results were compared with those of the stationary and random modes.

Related Studies

Thickness Measurement Technique

Measuring the thickness is an important factor in producing nanofiber filters. Previous studies have measured the thickness using thickness gauges, by direct contact or through optical microscopes by cross sectioning the nanofiber filter. A more accurate way is the bake–cut–microscope-measuring method [9]. First, the nanofiber filter was embedded in the resin to protect the nanofiber filter. Afterward, the resin-embedded nanofiber filter was cross-sectioned, and the thickness was measured by using an optical microscope. Although these methods could provide an accurate thickness of the nanofiber filter, they could damage the nanofiber filter and degrade its functions. Furthermore, the thickness could be only measured after the fabrication of the nanofiber filter.

Control in the Deposition of Electrospun Nanofibers

Several studies have been conducted to control the deposition of electrospun nanofibers. These studies have primarily used external forces such as electrostatic force by manipulating the electric field [30, 31], magnetic force by placing

permeant magnets, and mechanical force by using a rotating drum [6, 32] to achieve the controlled deposition of electrospun nanofibers. Although these methods have been proven successful in producing patterned or aligned nanofiber filters [33–35], the chaotic motion of electrospinning still hindered the production of a uniform-thickness nanofiber filter. By decreasing the voltage and reducing the distance between the syringe needle and metal collector, several studies have successfully reduced the bending instability [36] of the jet through near-field electrospinning [37, 38] and direct-write electrospinning [39]. However, these electrospinning methods have low productivity and produce extremely thin nanofiber filters, which cannot be utilized as an air filter.

Background

Reinforcement Learning

RL [40] is a type of ML algorithms for training an agent, interacting with the environment. RL primarily consists of an agent and environment; the agent (learner) dynamically interacts with the environment and obtains a reward based on its state. The agent selects an action a, which is the movement of the movable collector, based on the information about the state s in the environment at the current time t. At a subsequent time $t+1$, the agent receives a reward r_t, and the state s is changed to a new state (next state) s' as a result of the action a. At each time, the agent follows a policy π, which maps the state to the action to maximize the cumulative reward. The policy that maximizes the cumulative reward is called the optimal policy π^*, and RL is a sequential decision-making process that finds the optimal policy π^* through a series of interactions between the agent and the environment.

In this study, the RL algorithm that is trained to minimize the thickness variation of an electrospun nanofiber filter was adopted. The RL algorithm assumed the electrospinning process as the environment, and the state s was calculated on the basis of the measured thickness of the nanofiber filter. The agent of the RL algorithm manipulated the position of the movable collector (action, a) based on the optimal policy for the minimization of the thickness variation of the nanofiber filter.

Double Deep *Q*-Network

Model-free RL algorithms that could identify the optimal policy can be divided into value function-based [41] and policy-based approaches. This study used a value function-based approach of deep *Q-network* that achieved human-level control of Atari games [24]. The deep *Q-network* is grounded by training an agent based on an action-value function that provides the expected discounted return R_t for an action a with the environment of state s. The expected discounted return R_t is defined as $R_t = \sum_{k=t}^{\text{end}} \gamma^{k-t} r_k$ with a discount factor of $\gamma \in [0, 1]$. In this study, the discount factor was set to 0.99. The action-value function, also called known as the Q-function $Q(s, a)$ (Eq. 1), represents the expected utility of action a at a state s following policy π:

$$Q^{\pi}(s, a) = E\left[R_t | S_t = s, A_t = a\right]. \tag{1}$$

The optimal action is $a = \text{argmax}_{a \in A} Q^*(s, a)$. In dealing with the high-dimensional or continuous state space, a deep neural network was utilized to approximate the Q-function as follows: $Q(s, a) = Q(s, a; \theta)$, where θ is a parameter vector of the approximator. In estimating this network, we used Q-learning with double deep neural networks of the main *Q-network* $Q(s, a; \theta)$ and target *Q-network* $\hat{Q}(\text{s, a; } \theta^-)$, which is called known as double deep Q-learning or DDQN [42]. In estimating the DDQN, the main network $Q(s, a; \theta)$ is updated by minimizing the loss function $L_i\left(\theta_i\right)$ (Eq. 2) and using the stochastic gradient descent method at iteration i:

$$L(\theta) = \text{E}_{s,a,r,s'}\left[\left(r + \gamma \max_{a'} \hat{Q}\left(s', a'; \theta^-\right) - Q(s, a; \theta)\right)^2\right]. \tag{2}$$

Given that the rapid fluctuation of the Q-function $Q(s, a)$ often causes instability, the target network is frozen when updating the main network over a given k time steps and updated at every k time steps by copying the parameter of the main network to that of the target network ($\theta^- = \theta$). During the learning process, the ε-greedy method [43] was utilized to balance exploration and exploitation, where the agent selects the action with the greatest estimated value with a probability of $1 - \varepsilon$ (exploitation) and random actions with a probability of ε (exploration). Furthermore, the experience replay technique [44] was adopted to reduce the overfitting of a local region of the state space. This technique stores previous experiences in a replay buffer, and the update of the main network is performed using a uniformly sampled mini-batch from the replay buffer.

Methodology

Real-Time Thickness Measurement Technique

Real-time thickness measurements were performed on the basis of the previously reported system [45]. The flat LED plate on top of the chamber illuminated the uniform light to the nanofiber filter on the collector. Two cases of light intensity with and without passing through the nanofiber filter were measured by the CCD camera placed at the bottom of the collector. In calculating the light transmittance

of the nanofiber filter, the light intensity passing through the nanofiber filter was divided by the measured light intensity without the nanofiber filter. The light transmittance was converted into the thickness of the nanofiber filter based on the Beer–Lambert law (Eq. (3)).

$$T = e^{-\mu h}, \tag{3}$$

where T is the light transmittance, and h is the thickness of the nanofiber filter. Based on the Beer–Lambert law and calculated light transmittance at each pixel, the thickness of the nanofiber filter was evaluated using Eq. (4):

$$h(x) = -\ln T(x)/\mu, \tag{4}$$

where x is the x-axis position of the nanofiber filter corresponding to the pixel of the bottom image from the CCD camera, and $h(x)$ is the thickness of the nanofiber filter at position x. Although the y-axis variation of the thickness can be detected from this measurement system, the thickness of the nanofiber filter fabricated on the basis of a two-parallel-metal-plate collector varied only along the x-axis. Thus, the thickness was assumed as a function of the x position.

In the validating the real-time thickness measurement technique, the thickness of the nanofiber filter was measured by the bake–cut microscope-measuring method [9]. The nanofiber filter was immersed in a mixture of polydimethylsiloxane (PDMS) monomer and curing agent at a weight ratio of 10:1 and baked in a dry oven for 24 h at 40 °C. The PDMS-embedded nanofiber filter was cut along the x-axis to measure the thickness based on the cross-sectional image by using a microscope (Olympus BX53F2, Olympus, Japan).

The proposed real-time thickness measurement based on light transmittance could be applied to the translucent or light-transmitting materials; thus, it could be applied to all sorts of materials/electrospinning processes. However, considering that most of the electrospun nanofiber filters have high porosity and thin thickness, this measurement technique could be widely utilized for electrospun nanofiber filters.

Formulation of DDQN

A model-free RL framework of DDQN was implemented in the nanofiber filter production system to produce a nanofiber filter with a uniform thickness, namely, E-RL. Figure 1 illustrates the framework of the E-RL. The DDQN in the E-RL was trained to find the optimal policy based on the states, actions, and rewards. The DDQN was structured as a deep neural network with the parameters listed in Table 1. The action of the RL was set to the movement of the collector. Although the collector movement has a continuous action space, the

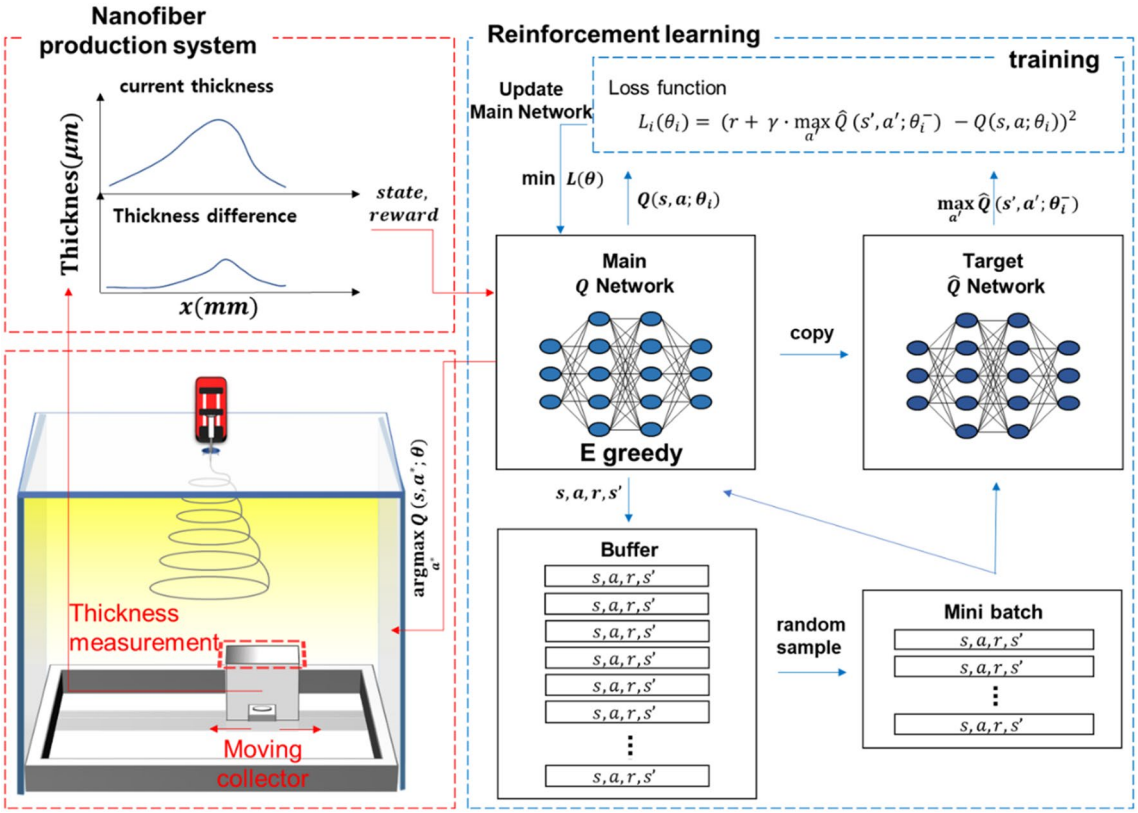

Fig. 1 Illustration of the DDQN-based nanofiber filter production framework (E-RL)

Table 1 Structure of the network

Layer	Number of neurons per layer	Activation
Input layer	2×890	Relu
Hidden layer 1	1024	Relu
Hidden layer 2	256	Relu
Drop out		
Batch normalization		
Hidden layer 3	256	Relu
Hidden layer 4	128	Relu
Drop out		
Batch normalization		
Hidden layer 5	128	Relu
Hidden layer 6	64	Relu
Hidden layer 7	32	Relu
Output layer	11	Softmax

movement of the collector was defined as a discrete action space to simplify the E-RL. We found that if RL has a large number of possible actions, then a single action generally moves the movable collector with a small distance, which does not effectively change the deposition behavior of the nanofiber filter for the generation of the uniform-thickness nanofiber filter. In addition, if RL possesses a small number of possible actions, then the distance gap between the possible actions is too large to move the movable collector to the desired position. Thus, to alleviate the non-uniformity of the nanofiber filter, an action space of the movable collector was set 11 equally spaced positions through trial and error. The states of the RL were designed on the basis of the thickness of the nanofiber filter and the difference between the current thickness and the previous thickness before the one step. The thickness of the nanofiber filter provided the information about the non-uniformity of the nanofiber filter. Moreover, the thickness difference provided the information about the deposition behavior of electrospun nanofibers. Based on the current state and action, the immediate reward, $r(s)$, is defined using Eqs. (5) and (6).

$$\text{if} \quad \mathbb{E}\left[h_s(x)\right] < h_t, \quad r(s) = \begin{cases} 1 - \text{var}\left[h_s(x)\right] \\ -h_t^2/N, \end{cases} \quad \text{if} \quad 1 - \text{var}\left[h_s(x)\right] < 0\ , \tag{5}$$

$$\text{if} \quad \mathbb{E}\left[h_s(x)\right] > h_t, \quad r(s) = \begin{cases} 1 - \text{var}\left[h_s(x) - h_t\right] \\ -1, \end{cases} \quad \text{if} \quad 1 - \text{var}\left[h_s(x) - h_t\right] < 0\ , \tag{6}$$

where $h_s(x)$ is the current thickness of the nanofiber filter in the state s; h_t is the target thickness of the nanofiber filter, and N represents the maximum possible number of steps that can be taken in one episode. In the case of the target thickness of 10 μm, the maximum possible number of steps, N, was set to 1000. The reward system was designed as follows. During the nonterminal state $\left(\mathbb{E}\left[h_s(x)\right] < h_t\right)$, a reward of $r(s) = 1 - \text{var}\left[h_s(x)\right]$ was assigned, and if $\text{var}\left[h_s(x)\right]$ was higher than 1, then the reward of $r(s) = -h_t^2/N$ was assigned as a penalty for the unnecessary increase in the total steps. At the terminal state when the average current thickness $\mathbb{E}\left[h_s(x)\right]$ in the state s exceeds the target thickness h_t, a terminal reward is assigned, exhibiting the highest value of 1 when the current and target thicknesses are exactly the same and decreasing by the variance of the difference between $h_s(x)$ and h_t. In addition, if the variance of the difference between $h_s(x)$ and h_t is higher than 1, then the fabricated nanofiber filter is considered non-uniform, and the terminal reward is assigned as − 1. As the variance of the difference between $h_s(x)$ and h_t decreases, the thickness of the nanofiber filter becomes more uniform, and the reward reaches 1.

Numerous electrospinning over 100,000 times is required to train RL. Considering that a single electrospinning process takes around 30 min, the training of the RL through experiments needs 50,000 h (around 6 years). Thus, as a method to dramatically reduce the time required for training the RL, production simulator software was developed. The production simulator software was designed on the basis of the empirical model of the deposition behavior of electrospun nanofibers on the two-parallel-metal-plate collector. The production simulator software was used to collect datasets consisting of s, a, r, and s' for training, and they were saved in the replay buffer before the training. During training, the mini-batch was randomly selected from the replay buffer to calculate the loss function. In evaluating the loss function, the mini-batch was used to calculate $Q\left(s, a; \theta_i\right)$ in the main *Q-network* and $\max_{a'} \hat{Q}\left(s', a'; \theta_i^-\right)$ in the target *Q*-network. Subsequently, the main *Q-network* is updated by minimizing the loss function by using the gradient descent method with a learning rate α of 0.00025. The learning rate is defined as the size of a gradient descent step. However, considering that the optimal policy is not derived with only one step of training, the dataset collection and training process were repeated until the optimal policy was obtained (Fig. 1).

Experimental Sections

Nanofiber Filter Production System

The schematic and photograph of the nanofiber filter production system are shown in Fig. 2a, b, respectively. The detailed configuration of the proposed nanofiber filter production system, which is similar to our previous study [45], includes a nanofiber generation system, movable

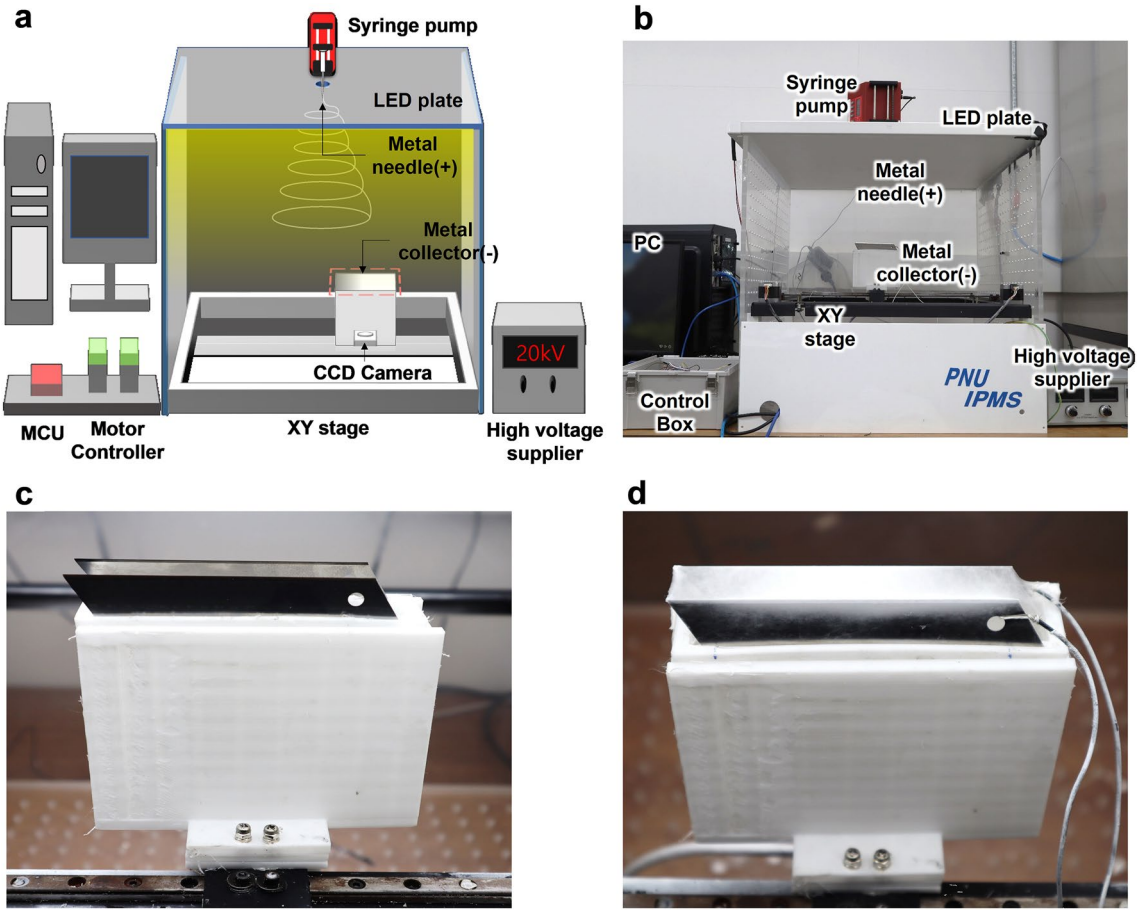

Fig. 2 **a** Schematic and **b** photograph of E-RL. Photograph of a movable two-parallel-metal collector without (**c**) and with nanofiber filter (**d**)

metal collector, and real-time thickness measurement system. The nanofiber generation system has a configuration similar to that of the conventional electrospinning of a syringe pump (NE300, New Era, USA), a 3 mL plastic syringe with a 23-gauge metal needle, a high-voltage supplier (HV30, NanoNC, South Korea), and an electrospinning chamber. Its key feature is the movable metal collector composed of a two-parallel-metal-plate collector with a 3 cm width, a 3D-printed collector holder, and an automatic *XY* stage. The movable collector is shown in Fig. 2c, d. The width of a two-parallel-metal-plate collector could be larger as shown in Fig. S3. Because the electrospinning time was exponentially increased as widening the width of the nanofiber filter, the effective width for the two-parallel-metal-plate collector would be below several centimeters. The real-time thickness measurement system consists of a flat LED plate located on top of the electrospinning chamber and a CCD camera (oCam-1CGN-U-T, WITHROBOT, South Korea) located below the movable collector.

Nanofiber Filter Production

Nanofiber filter production was conducted on the basis of a previous study [46]. Gelatin from bovine skin (type B, Sigma-Aldrich, USA), polycaprolactone (PCL) pellets (Mn = 80,000 g mol^{-1}, Sigma-Aldrich, USA), 2,2,2-trifluoroethanol (TFE), and acetic acid were used for PCL/gelatin solutions. 10% w/v PCL/TFE and 10% w/v gelatin/TFE were prepared, and then the solutions were mixed in a 50:50 mass ratio with 10 µL of acetic acid (0.1% of TFE). The mixed solutions were stirred for 12 h prior to processing to ensure thorough mixing. The PCL/gelatin solution was placed in a 3 mL plastic syringe with a 23-gauge metal needle and ejected through the metal needle at a constant flow rate of 0.5 mL h^{-1} using a syringe pump. After connecting a (+) electrode to a metal needle and a (−) electrode to the movable collector, 20 kV was applied between the two electrodes to deposit the nanofibers on the movable collector and form a nanofiber filter. When a high voltage is applied

between the metal needle and the movable collector, a Taylor cone is induced at the tip of the metal needle, and a polymer jet is ejected from the tip of the Taylor cone. Given the high voltage, the polymer jet carries a high surface charge, causing electrostatic repulsion and bending instability. Its diameter is decreased to the nanoscale by electrostatic repulsion and solvent evaporation, thereby forming nanofibers. The bending instability causes the nanofibers from the polymer jet to be randomly deposited on the collector. Consequently, if the movable collector is stationary, then the nanofiber filter has been frequently produced with a non-uniform thickness.

Production Simulation Software

The simulator software was developed on the basis of the empirical model of the deposition behavior of electrospun nanofibers on the two-parallel-metal-plate collector. The deposition behavior was assumed to be a Gaussian distribution with an altering center and a standard deviation [45]. By empirically acquiring the parameters for the altering center and standard deviation of the Gaussian distribution, the software simulated the deposition of a nanofiber filter produced by the nanofiber filter production system, thereby generating a bottom-view image of the nanofiber filter similar to that from a CCD camera. The light transmittance calculated using the bottom-view image was converted into thickness using the Beer–lambert law.

Performance Evaluation of the E-RL

After training the simulation software, the DDQN model was transferred to the production simulation software and E-RL with a target thickness of 10 μm. The performance of the E-RL was numerically and experimentally confirmed by comparing it with the stationary and random modes. In the stationary mode, the collector accumulated electrospun nanofibers in a fixed center position without any movement. In the random mode, the collector moved in random directions during electrospinning. Finally, in the DDQN mode, the collector moved in accordance with the optimal action obtained from the trained DDQN model based on the measured thickness of the nanofiber filter.

Air Filtration

The air filtration efficiency of the nanofiber filter fabricated through electrospinning was measured at four positions: first, second, third, and fourth of the nanofiber filter. Incenses were burned to generate aerosol particles, and the existence of PM2.5 was confirmed by using optical particle size (Model-3330, TSI) as shown in Fig. S4. The PM particles, which were produced by burning incense, flowed from the right to the left beaker and then filtered at each position of the nanofiber filter. In measuring the concentration of incident and filtered PM2.5, laser particle sensors (PM2008, CUBIC, China) were positioned in the right and left beakers.

Results and Discussion

Nanofiber Filter Production

Electrospinning on a two-parallel-metal-plate collector produced nanofiber filter on and in-between two metal plates. Figure 3a shows the bottom-view image of the nanofiber filter obtained using the CCD camera. The bright region of the bottom-view image showed high light transmittance and low thickness, whereas the dark region showed a lower light transmittance and thicker nanofiber filter. Thus, the gradation of the color of the bottom-view images indicates the non-uniform thickness of the nanofiber filter. Given that the two-parallel-metal-plate collector generally produced aligned nanofiber filters [47], the variation of the light transmittance and thickness in the *y*-axis direction would be negligible. Thus, the thickness of the nanofiber filter was simplified as a function of the *x*-axis position. Due to the bending instability and varying jetting direction of the multiple modes of jet, the deposition behavior of electrospun nanofibers was inconsistent as shown Fig. S5. Such inconsistent deposition behavior would not be easily modeled by conventional control theory, and thus, the RL algorithm was adopted to control the deposition of electrospun nanofibers. Figure 3b shows the conversion of light transmittance to the thickness of the nanofiber filter using the Beer–Lambert law along the *x*-axis. The nanofiber fabrication of the nanofiber filter production system was confirmed through the SEM image of the nanofiber filter (Fig. 3c).

Real-Time Thickness Measurement System

In measuring the thickness of the nanofiber filter, many studies embedded the nanofiber filter in PDMS and measured the thickness of the nanofiber filter from the cross-sectional view [9]. However, the embedding process damaged the nanofiber filter and hindered its utilization as a porous membrane for air/liquid filter, battery separator, and biomedical scaffold. As a non-destructive technique, the transmitted light through the nanofiber filter was measured and converted into the thickness of the nanofiber mat based on the Beer–Lambert law, which states the relationship between the attenuation of light and thickness of the medium (Fig. 3d). For simplification, the nanofiber filter was assumed as a homogenous medium. By fitting a curve to the measured data of the light transmittance and the thickness (Fig. 3e), we calculated the

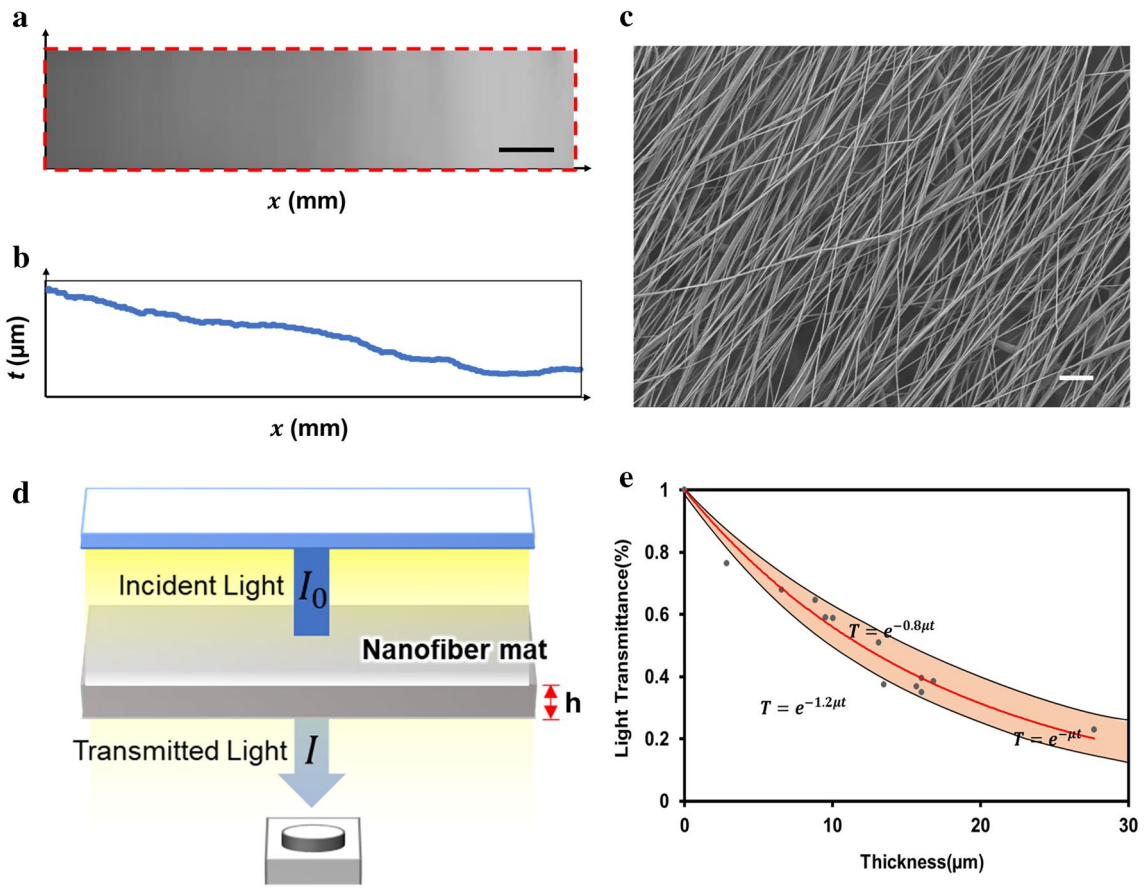

Fig. 3 **a** Bottom-view image of the nanofiber filter, the scale bar indicates 1 cm, and **b** is converted to the thickness of the nanofiber filter along the *x*-axis by Beer–Lambert law. **c** SEM image of nanofiber filter. The scale bar indicates 10 μm. **d** Schematic for real-time thickness measurement based on Beer–Lamber law and **e** Curve of the light transmittance versus the thickness of nanofiber filter

attenuation coefficient μ of 0.058 μm^{-1}. Approximately, 83% of the measured thickness data were in the area with a ± 20% deviation of μ (Fig. 3e). When the thickness of the nanofiber mat became 30 μm, the resolution was around 0.77 μm because the CCD camera has an image depth of 8-bit. When a higher-bit depth CCD camera and brighter light source are used, higher resolution in the thickness measurement can be achieved even with thicker nanofiber filter.

Changes in electrospinning parameters such as applied voltage, flow rate, viscosity, solvent, solution concentration, temperature, and humidity influence the property of electrospun nanofibers such as diameter, density, and porosity, and affect the transmission of light through the nanofiber filters. The attenuation coefficient of the Beer–Lambert law was determined based on the property of electrospun nanofibers. Thus, by finding an appropriate attenuation coefficient for each solvent, the thickness of the nanofiber filter produced with different solvents would be estimated based on the Beer-Lambert law.

Training of the DDQN

The computer consisted of Intel® Core™ i5-8500 CPU @ 3.00 GHz and NVIDIA GeForce RTX3060 GPU. The RL algorithm was achieved with Python version 3.8.10. under the visual studio code framework. The training process was repeated 100,000 times and took around 4 days. In evaluating the uniformity of a produced nanofiber filter during training, the terminal variance, which is the variance between the target thickness and the current thickness at the end of the fabrication, was introduced. The terminal variance was negatively correlated with the non-uniformity of the nanofiber filter thickness. When the thickness of the nanofiber filter is the

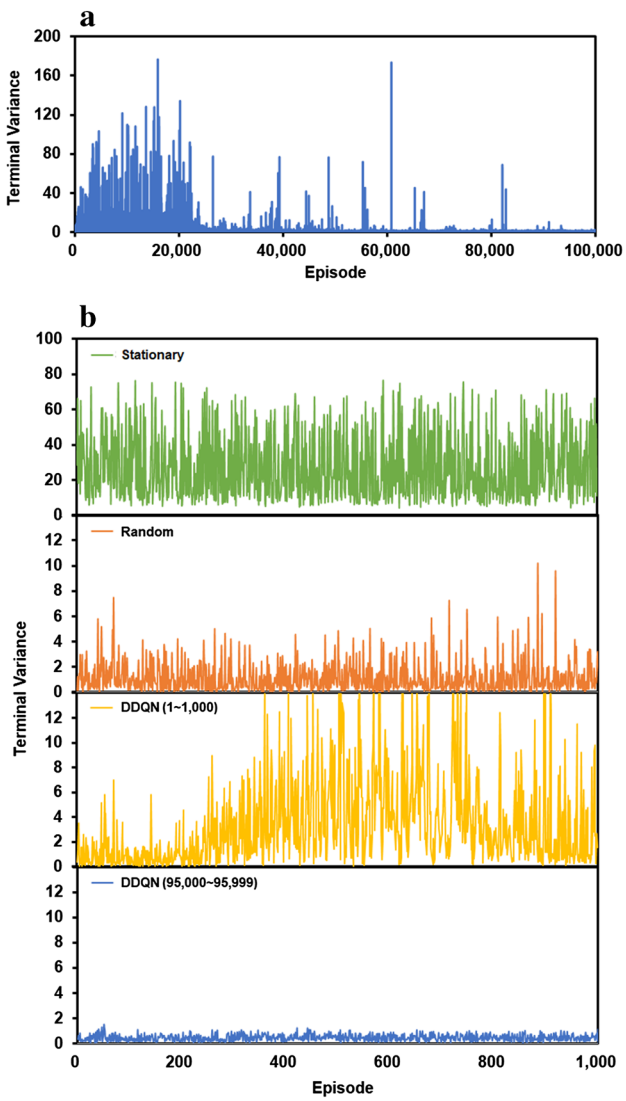

Fig. 4 **a** Terminal variance for the DDQN mode. **b** Terminal variance for stationary mode, random mode, and untrained (1–1000 episode) and trained DDQN mode (from 95,000 to 95,999 episodes) with respect to episodes

same as the target thickness and perfectly uniform, the terminal variance becomes 0. However, as the non-uniformity of the nanofiber filter increases, the terminal variance increases by the amount of variance between the target and the current thickness of the nanofiber filter. Figure 4a, b shows the change in terminal variance in the case of stationary, random, and DDQN modes during training. The training of DDQN was conducted as the episode processed (Fig. 4a). As shown in Fig. 4a, in the beginning of the training process, the high value of the terminal variance was observed, but low terminal variance was consistently achieved after 95,000 episodes because of continuous training. The terminal variance of the sufficiently trained DDQN mode (from 95,000 to 95,999 episodes) was compared with that of the other modes (Fig. 4b). In the stationary mode, the terminal variance was maintained at a high value throughout all the episodes. In the random mode, the terminal variance fluctuated between the high terminal variance of the stationary mode and the low terminal variance of the sufficiently trained DDQN mode. However, the random mode could hardly ensure the reliability of the uniformity of the nanofiber filter thickness because the terminal variance significantly varied at each episode. In contrast, the trained DDQN mode produced uniform-thickness nanofiber filters with a low terminal variance during more than 1000 episodes. This result demonstrated that the E-RL has a superior ability to produce a uniform nanofiber filter, validating the effectiveness of the DDQN to determine the optimal policy (Fig. S6).

DDQN-Based Simulation Model

After transferring the trained DDQN to the nanofiber production simulation software, the performance of DDQN mode was verified by comparing it with the stationary and random modes. Figure 5 shows the bottom-view image of the nanofiber filter generated by the numerical simulation with and without DDQN. In the stationary mode, the bottom-view images of the nanofiber filter show enlarged gradation as the number of steps increased, which indicates that electrospun nanofibers were non-uniformly accumulated on the collector (Fig. 5a). In the random mode, the gradation of the bottom-view images of the nanofiber filter was slightly alleviated compared with that of the stationary mode (Fig. 5b). In the DDQN mode, the bottom-view images of the nanofiber filter show a high level of uniformity throughout all the steps (Fig. 5c). These results indicated that the DDQN mode exhibited superior performance in producing a uniform-thickness nanofiber filter.

For quantitative analysis, Fig. 5d, e shows the standard deviation and normalized squared error (NSE) with and without DDQN. The degree of uniformity was determined using the standard deviation value of the nanofiber filter. In the stationary mode, the standard deviation continuously increased at the highest rate. In the random mode, the increased rate of the standard deviation was lower than that of the stationary mode, but it eventually increased. In the DDQN mode, the standard deviation was lower and steadier than that in the other two modes. The NSE in the three modes also showed similar trend of the standard deviation results. The NSE decreased at a similar rate before approximately 60 steps for all cases. However, in the stationary mode, the decrease of the NSE eventually stopped, and the NSE increased after approximately 60 steps. In the random and DDQN modes, the NSE continuously decreased until the end of the episode. However, in the random mode, the terminal value was higher than that of the DDQN mode.

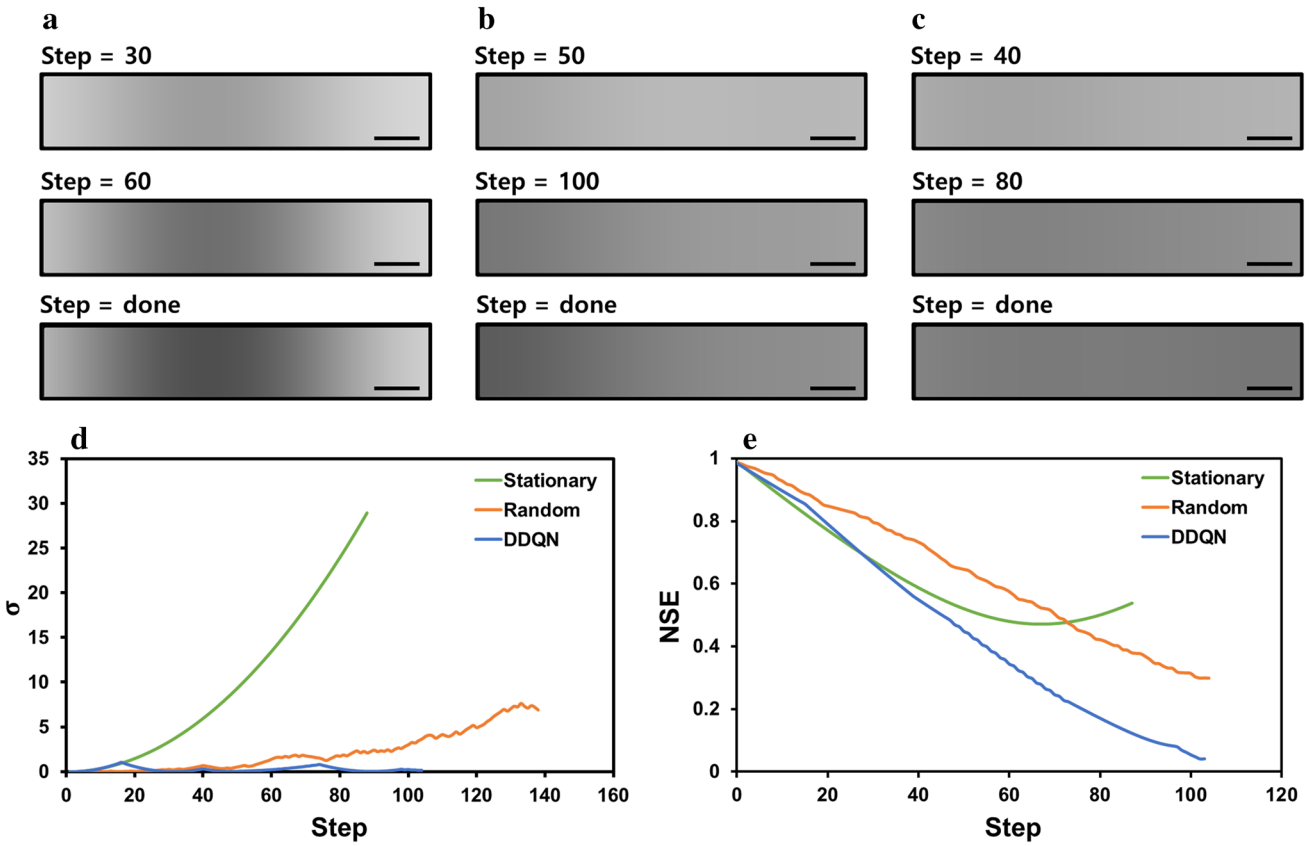

Fig. 5 Performance evaluation of the simulation model. Bottom-view images of the stationary mode (**a**), random mode (**b**), and DDQN mode (**c**). **d** Comparison of the standard deviation (σ) and **e** normalized squared error (NSE) between the three modes. All scale bars indicate 1 cm

Adaptive Electrospinning System for Uniform-Thickness Nanofiber Filter

The performance of the DDQN mode was experimentally validated by the transfer learning of the trained DDQN into the electrospinning system, namely, E-RL. Figure 6 shows the bottom-view images experimentally obtained from the nanofiber filter production system in the stationary, random, and DDQN modes. The experimental results from the nanofiber filter production system showed a similar trend as that of the numerical simulation. In the stationary mode, the bottom-view images of the nanofiber filter exhibited the highest non-uniform gradation throughout all the steps (Fig. 6a). In the random mode, the bottom-view images showed a non-uniform gradient, but they were slightly more uniform than in the stationary mode (Fig. 6b). In the DDQN mode, the bottom-view images of the nanofiber filter showed a high level of uniformity regardless of the step (Fig. 6c).

Figure 6d shows the standard deviation of the thickness of the nanofiber filter produced based on the stationary, random, and DDQN modes. In the stationary mode, the standard deviation was continuously increased, and it showed the highest value at the end of the step. In the random mode, although the standard deviation values slightly decreased, it showed a higher trend than the DDQN mode. In the DDQN mode, the standard deviation was continuously lower than 1. At the end of the steps, the standard deviation of the nanofiber filter thickness with the DDQN mode was approximately five times lower than that of the stationary mode and two times lower than that of the random mode. Figure 6e shows a graph of the NSE for the three modes. In the stationary mode, the NSE initially decreased and gradually saturated at a certain value. In the random and DDQN modes, the NSE continued to decrease at a similar rate. However, the NSE of the random mode was higher than that of the DDQN mode similar to the results obtained from the simulation model. The NSE ultimately decreased five times lower in the DDQN mode compared with the stationary mode and two times lower than the random mode, which indicates that the E-RL showed an outstanding ability to produce a uniform nanofiber filter.

The production performance of a uniform-thickness nanofiber filter could be explained by the following reasons. In the stationary mode, the nanofibers largely accumulated in a narrow area of the collector following a Gaussian distribution. In the random mode, the nanofiber filter thickness

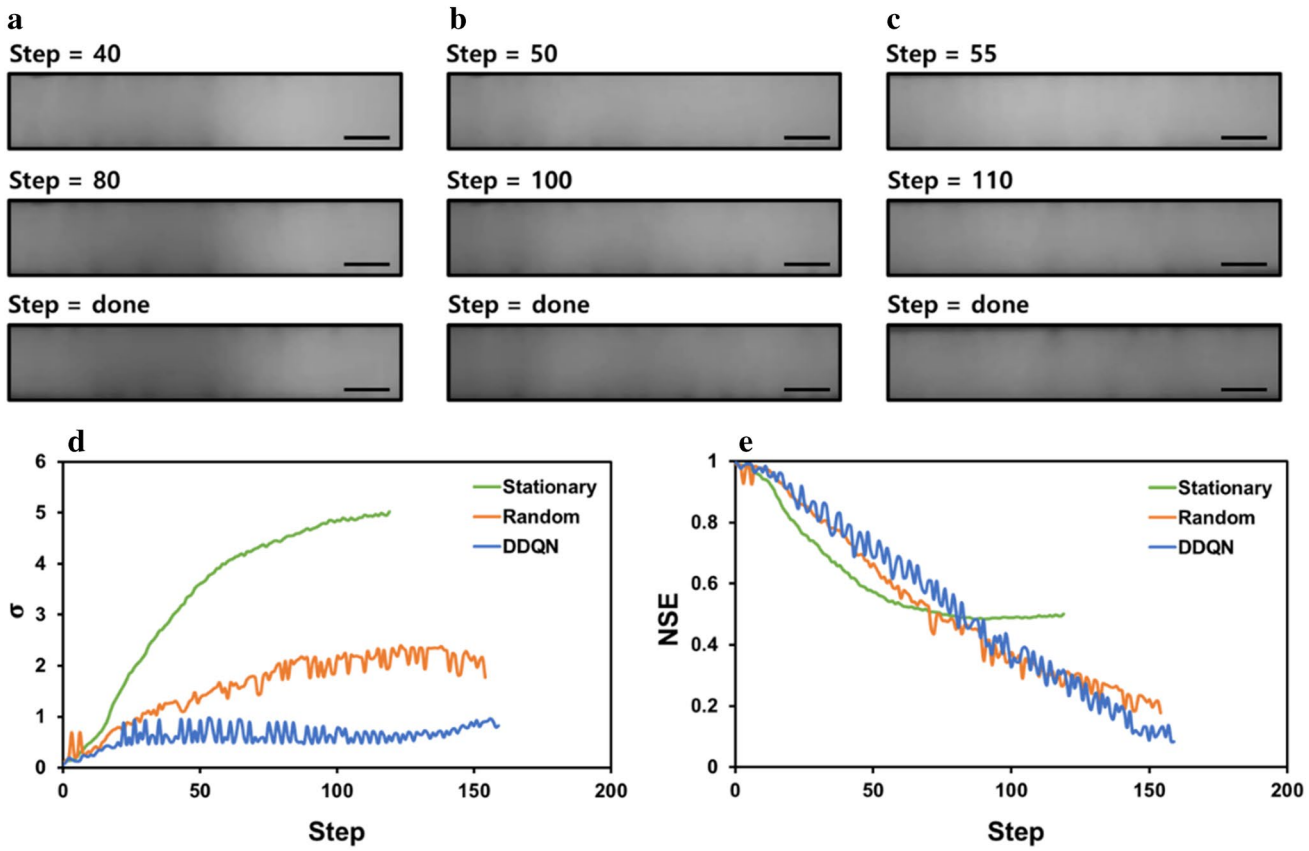

Fig. 6 Performance evaluation of the nanofiber filter production in real time during electrospinning. Bottom-view images of the stationary mode (**a**), random mode (**b**), and DDQN mode (**c**). **d** Comparison of standard deviation (σ) and **e** normalized squared error (NSE) between the three modes. All scale bars indicate 1 cm

was slightly more uniform than that in the stationary mode because of the random movement of the collector. However, the nanofibers remained non-uniformly accumulated on the collector because the collector moved without a specific strategy. In the DDQN mode, the nanofibers were uniformly accumulated because the RL-based moving collector followed the optimal policy.

Air Filtration of the Nanofiber Filter

For comparison of three modes of the stationary, random and DDQN modes, an air filtration experiment was conducted. The air filtration experimental setup and schematic of the nanofiber filter with four positions are shown in Fig. 7a, b, respectively. The thickness and filtration efficiency at four positions with one-representative sample are presented in Fig. 7c. In the DDQN mode, the filtration efficiency at the four positions exhibited high and uniform performance, while in the other two modes, the filtration efficiency at the fourth position is much lower than that at the other three positions. By comparing the thickness of each position and the filtration efficiency, we confirmed that the uniformity of the thickness of the nanofiber filter affects the uniformity of the filtration efficiency for each position. Figure 8 shows the standard deviation of thickness and filtration efficiency among four positions for each mode. The standard deviation of thickness among four positions for the DDQN, random, and stationary mode was 0.747, 1.386, and 3.608, respectively. The standard deviations of the filtration efficiency for the three modes were 2.004, 11.5, and 22.552, respectively. The standard deviation of the filtration efficiency of the DDQN mode was approximately 5.74 and 11.3 times lower than that of the random and stationary mode, respectively. This result indicated that the non-uniform thickness of the nanofiber filters produced with the stationary and random modes detrimentally affected the filtration efficiency. Furthermore, the thickness difference causes the flow concentration toward the thin–thickness region that showed low filtration efficiency and rapid degradation in filtration performance of the nanofiber air filter. Thus, the suggested E-RL is effective in producing a uniform nanofiber filter for the uniform performance of the air filter. Furthermore, apart from the uniformity, the E-RL produces electrospun

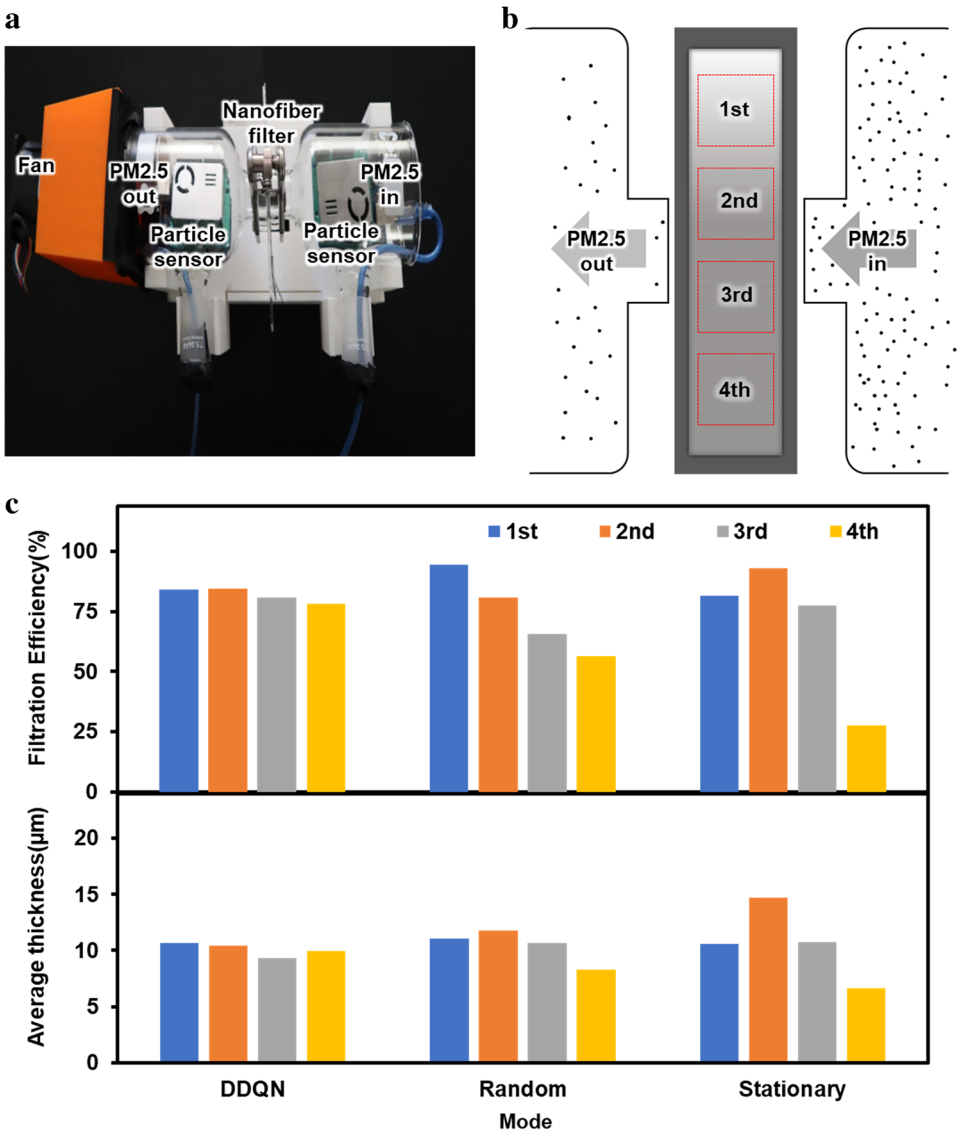

Fig. 7 **a** Photograph of the setup of the filtration experiment and **b** schematic of the nanofiber filter test. **c** The filtration efficiency and thickness at the first, second, third, and fourth positions for the stationary, random, and DDQN mode

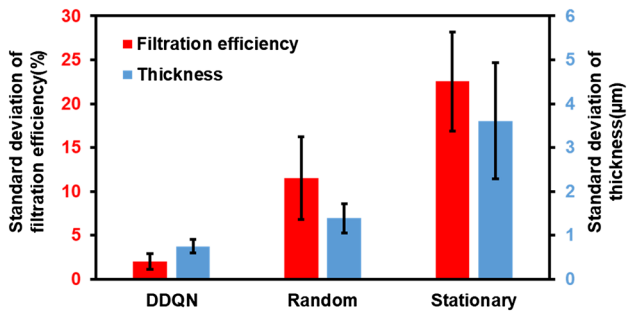

Fig. 8 Standard deviation of the thickness and filtration efficiency

nanofiber filters with superior air filtration, considering that many previous studies on nanofiber filters have shown high-efficiency air filtration.

Conclusion

In this study, E-RL was developed to produce uniform-thickness nanofiber filters. The E-RL accomplishes the real-time measurement of thickness by using the Beer–Lambert law, which has an exponential relationship between light transmittance and thickness. Using the production simulation

software, the training process could be accelerated, and the DDQN was trained to determine the optimal policy, which was the movement strategy for the collector to minimize the standard deviation and NSE of the thickness uniformity. The trained DDQN model was applied to the production simulation software and E-RL. Consequently, the uniformity in the thickness of the nanofiber filter was evidently improved for both cases—production simulation software and E-RL. Therefore, the E-RL is expected to greatly improve the productivity and reliability of the nanofiber filter.

E-RL was applied to electrospinning with a two-parallel-metal-plate collector, which could be simplified into the 1D case. For application to a wider range of industries and research fields, the scaling up is one of the important issues of E-RL. However, applying the real-time thickness measurement to larger collectors, such as 2D metal collectors, is extremely difficult. One way to overcome such limitations is the implementation of a transparent collector, such as a transparent film (e.g., ITO film), metal mesh collector, and an electrolyte solution, to achieve real-time thickness measurement of 2D nanofiber filters for E-RL. By adopting this idea, E-RL could be incorporated with the electrospinning process on a larger transparent collector. Furthermore, the transparent film or metal mesh is expected to be applied to scaled-up electrospinning system such as a continuously running conveyor belt and a needless spinning system. Considering the wide utilization of electrospun nanofiber filters, the implementation of the E-RL to the scaled-up electrospinning system will have a broad impact in the field of electrospinning and related application in both industries and research.

Supplementary Information The online version contains supplementary material available at https://doi.org/10.1007/s42765-022-00247-3.

Acknowledgements This work was supported by the National Research Foundation of Korea (NRF) Grant funded by the Korea government (MSIT) (No. 2020R1C1C1009443) and has been conducted with the support of Korea Institute of Industrial Technology as Development of intelligent root technology with add-on modules (KITECH EO-22-0005).

Data availability The data that support the findings of this study are available from the authors upon reasonable request.

Declarations

Conflict of interest The authors state that there are no conflicts of interest to disclose

References

1. Huang ZM, Zhang YZ, Kotaki M, Ramakrishna S. A review on polymer nanofibers by electrospinning and their applications in nanocomposites. *Compos Sci Technol* **2003**;*63*:2223.
2. Li D, Xia Y. Electrospinning of nanofibers: Reinventing the wheel? *Adv Mater* **2004**;*16*:1151.
3. Sun B, Long YZ, Zhang HD, Li MM, Duvail JL, Jiang XY, Yin HL. Advances in three-dimensional nanofibrous macrostructures via electrospinning. *Prog Polym Sci* **2014**;*39*:862.
4. Zhu J, Jiang S, Hou H, Agarwal S, Greiner A. Low density, thermally stable, and intrinsic flame retardant poly(bis(benzimidazo) benzophenanthroline-dione) sponge. *Macromol Rapid Commun* **2018**;*303*:1.
5. Xu J, Liu C, Hsu P-C, Liu K, Zhang R, Liu Y, Cui Y. Roll-to-roll transfer of electrospun nanofiber film for high-efficiency transparent air filter. *Nano Lett* **2016**;*16*:1270.
6. Gu GQ, Han CB, Lu CX, He C, Jiang T, Gao ZL, Li CJ, Wang ZL. Triboelectric nanogenerator enhanced nanofiber air filters for efficient particulate matter removal. *ACS Nano* **2017**;*11*:6211.
7. Choi SW, Jo SM, Lee WS, Kim YR. An electrospun poly(vinylidene fluoride) nanofibrous membrane and its battery applications. *Adv Mater* **2003**;*15*:2027.
8. Pham QP, Sharma U, Mikos AG. Electrospinning of polymeric nanofibers for tissue engineering applications: a review. *Tissue Eng* **2006**;*12*:1197.
9. Park SM, Kim DS. Electrolyte-assisted electrospinning for a self-assembled, free-standing nanofiber membrane on a curved surface. *Adv Mater* **2015**;*27*:1682.
10. Wu T, Ding M, Shi C, Qiao Y, Wang P, Qiao R, Wang X, Zhong J. Resorbable polymer electrospun nanofibers: history, shapes and application for tissue engineering. *Chin Chem Lett* **2020**;*31*:617.
11. Song JY, Ryu HI, Lee JM, Bae SH, Lee JW, Yi CC, Park SM. Conformal fabrication of an electrospun nanofiber mat on a 3D ear cartilage-shaped hydrogel collector based on hydrogel-assisted electrospinning. *Nanoscale Res Lett* **2021**;*16*:116.
12. Song JY, Kim DY, Yun HJ, Kim JH, Yi CC, Park SM. Electroconductive, flexible, and printable graphene nanoplate-carbon nanotube–polydimethylsiloxane composite collectors for three-dimensional conformal electrospinning. *Compos Sci Technol* **2022**;*227*:1.
13. Conte AA, Sun K, Hu X, Beachley VZ. Effects of fiber density and strain rate on the mechanical properties of electrospun polycaprolactone nanofiber mats. *Front Chem* **2020**;*8*:610.
14. Mahjour SB, Sefat F, Polunin Y, Wang LC, Wang HJ. Improved cell infiltration of electrospun nanofiber mats for layered tissue constructs. *J Biomed Mater Res Part A* **2016**;*104*:1479.
15. Liu C, Hsu PC, Lee HW, Ye M, Zheng GY, Liu NA, Li WY, Cui Y. Transparent air filter for high-efficiency PM2.5 capture. *Nat Commun* **2015**;*6*:1.
16. Abiodun OI, Jantan A, Omolara AE, Dada KV, Umar AM, Linus OU, Arshad H, Kazaure AA, Gana U, Kiru MU. Comprehensive review of artificial neural network applications to pattern recognition. *IEEE Access* **2019**;*7*:158820.
17. Pisner DA, Schnyer DM. Support vector machine. Machine learning. London: Elsevier; **2020**. p. 101.
18. Gou J, Ma H, Ou W, Zeng S, Rao Y, Yang H. A generalized mean distance-based *k*-nearest neighbor classifier. *Expert Syst Appl* **2019**;*115*:356.
19. Charbuty B, Abdulazeez A. Classification based on decision tree algorithm for machine learning. *J Appl Sci Technol Trends* **2021**;*2*:20.
20. Mahmood T. Generalized linear model based monitoring methods for high-yield processes. *Qual Reliab Eng Int* **2020**;*36*:1570.
21. Kim MJ, Song JY, Hwang SH, Park DY, Park SM. Electrospray mode discrimination with current signal using deep convolutional neural network and class activation map. *Sci Rep* **2022**;*12*:1.
22. Ahmed M, Seraj R, Islam SMS. The *k*-means algorithm: a comprehensive survey and performance evaluation. *Electronics* **2020**;*9*:1295.
23. Kobak D, Berens P. The art of using t-SNE for single-cell transcriptomics. *Nat Commun* **2019**;*10*:1.

24. Mnih V, Kavukcuoglu K, Silver D, Rusu AA, Veness J, Bellemare MG, Graves A, Riedmiller M, Fidjeland AK, Ostrovski G, Petersen S, Beattie C, Sadik A, Antonoglou I, King H, Kumaran D, Wierstra D, Legg S, Hassabis D. Human-level control through deep reinforcement learning. *Nature* **2015**;*518*:529.
25. Silver D, Huang A, Maddison CJ, Guez A, Sifre L, van den Driessche G, Schrittwieser J, Antonoglou I, Panneershelvam V, Lanctot M, Dieleman S, Grewe D, Nham J, Kalchbrenner N, Sutskever I, Lillicrap T, Leach M, Kavukcuoglu K, Graepel T, Hassabis D. Mastering the game of Go with deep neural networks and tree search. *Nature* **2016**;*529*:484.
26. Chen Y, Norford LK, Samuelson HW, Malkawi A. Optimal control of HVAC and window systems for natural ventilation through reinforcement learning. *Energy Build* **2018**;*169*:195.
27. Kober J, Bagnell JA, Peters J. Reinforcement learning in robotics: a survey. *Int J Robot Res* **2013**;*32*:1238.
28. Xu Y-H, Yang C-C, Hua M, Zhou W. Deep deterministic policy gradient (DDPG)-based resource allocation scheme for NOMA vehicular communications. *IEEE Access* **2020**;*8*:18797.
29. Swinehart DF. The beer-lambert law. *J Chem Educ* **1962**;*39*:333.
30. Angammana CJ, Jayaram SH. Investigation of the optimum electric field for a stable electrospinning process. *IEEE T Ind Appl* **2012**;*48*:808.
31. Song JY, Oh JH, Choi D, Park SM. Highly efficient patterning technique for silver nanowire electrodes by electrospray deposition and its application to self-powered triboelectric tactile sensor. *Sci Rep* **2021**;*11*:21437.
32. Katta P, Alessandro M, Ramsier RD, Chase GG. Continuous electrospinning of aligned polymer nanofibers onto a wire drum collector. *Nano Lett* **2004**;*4*:2215.
33. Zhang D, Chang J. Patterning of electrospun fibers using electroconductive templates. *Adv Mater* **2007**;*19*:3664.
34. Park SM, Eom S, Choi D, Han SJ, Park SJ, Kim DS. Direct fabrication of spatially patterned or aligned electrospun nanofiber mats on dielectric polymer surfaces. *Chem Eng J* **2018**;*335*:712.
35. Li D, Ouyang G, McCann JT, Xia Y. Collecting electrospun nanofibers with patterned electrodes. *Nano Lett* **2005**;*5*:913.
36. Reneker DH, Yarin AL, Fong H, Koombhongse S. Bending instability of electrically charged liquid jets of polymer solutions in electrospinning. *J Appl Phys* **2000**;*87*:4531.
37. Park YS, Kim J, Oh JM, Park S, Cho S, Ko H, Cho YK. Near-field electrospinning for three-dimensional stacked nanoarchitectures with high aspect ratios. *Nano Lett* **2020**;*20*:441.
38. Bisht GS, Canton G, Mirsepassi A, Kulinsky L, Oh S, Dunn-Rankin D, Madou MJ. Controlled continuous patterning of polymeric nanofibers on three-dimensional substrates using low-voltage near-field electrospinning. *Nano Lett* **1831**;*2011*:11.
39. Chen H, Malheiro A, van Blitterswijk C, Mota C, Wieringa PA, Moroni L. Direct writing electrospinning of scaffolds with multidimensional fiber architecture for hierarchical tissue engineering. *ACS Appl Mater Interfaces* **2017**;*9*:38187.
40. Sutton RS, Barto AG. Reinforcement learning: an introduction. London: MIT Press; **2018**.
41. Szepesvári C, Littman ML. A unified analysis of value-function-based reinforcement-learning algorithms. *Neural Comput* **2017**;*1999*:11.
42. Van Hasselt H, Guez A, Silver D, editors. Deep reinforcement learning with double *Q*-learning. Proc. Conf. AAAI Artif. Intell; 2016.
43. Thrun SB. Efficient exploration in reinforcement learning. London: Springer; **1992**.
44. Lin L-J. Self-improving reactive agents based on reinforcement learning, planning and teaching. *Mach Learn* **1992**;*8*:293.
45. Ryu HI, Koo MS, Kim S, Kim S, Park YA, Park SM. Uniform-thickness electrospun nanofiber mat production system based on real-time thickness measurement. *Sci Rep* **2020**;*10*:20847.
46. Park BU, Park SM, Lee KP, Lee SJ, Nam YE, Park HS, Eom S, Lims JO, Kim DS, Kim HK. Collagen immobilization on ultra-thin nanofiber membrane to promote in vitro endothelial monolayer formation. *J Tissue Eng* **2019**;*10*:1.
47. Li D, Wang Y, Xia Y. Electrospinning of polymeric and ceramic nanofibers as uniaxially aligned arrays. *Nano Lett* **2003**;*3*:1167.

Seok Hyeon Hwang is currently pursuing a M.S. under the supervision of Prof. Sang Min Park, Pusan National University. He started his academic studies in the field of Mechanical Engineering and received B.S. degree from Pusan National University, South Korea in 2021. His research interest is the artificial intelligence-based production systems.

Jin Yeong Song is currently pursuing a M.S. under the supervision of Prof. Sang Min Park, Pusan National University. He started his academic studies in the field of Mechanical Engineering and received B.S. degree from Pusan National University, South Korea in 2021. His research interest is based on 2D and 3D conformal electrospinning and its environmental applications for electrospun nanofiber air filters.

Hyun Il Ryu received M.S. degree from Pusan National University, South Korea in 2020. He started his academic studies in the field of Mechanical Engineering and received B.S. degree from Pusan National University. His research interest is the development of advanced nano/microfabrication techniques production system.

Jae Hee Oh received a B.S. under the supervision of Prof. Sang Min Park from Pusan National University, South Korea in 2021. He started his academic studies in the field of Mechanical Engineering from Pusan National University, South Korea. His research interest is based on fabricating technology of transparent electrodes and strain sensors.

Seungwook Lee is a research assistant and a Ph.D. candidate in the Nanoparticle Technology Laboratory, Pusan National University. He received B.S. in Mechanical and Automotive Engineering from Pukyong National University and M.S. degrees in Mechanical Engineering from Pusan National University. His research interests include experimental studies of nanoparticle deposition and semiconductor cleaning.

Donggeun Lee is a professor in the School of Mechanical Engineering and a head of the Nanoparticle Technology Laboratory, Pusan National University. He received Ph.D. degree in Mechanical Engineering from the Seoul National University. From 2001 to 2003, he was a research associate at Center for NanoEnergetic Research, University of Minnesota. He is a member of American Association for Aerosol Research and an editor of Advanced Powder Technology.

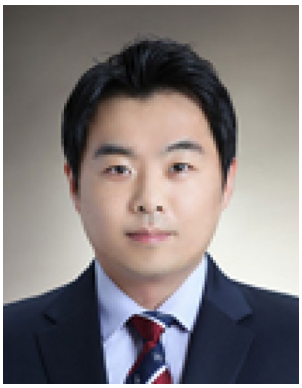

Dong Young Park is currently a senior researcher at Korea Institute of Industrial Technology (KITECH), South Korea. He worked at Korea Institute of Energy Research (KIER), South Korea. He received his B.S. degree from Pusan National University, South Korea. He achieved his M.S. and Ph.D. degrees in Department of Mechanical Engineering at Pohang University of Science and Technology (POSTECH), South Korea. His research fields of specialization and interest are quantification based on image processing for material characteristics and process optimization through artificial intelligence in industrial manufacturing.

Sang Min Park is an assistant professor at the School of Mechanical Engineering, Pusan National University, South Korea. He received his Ph.D. degree from Pohang University of Science and Technology (POSTECH) in 2018, by developing an electrolyte-assisted electrospinning technique for recapitulating the blood-tissue interfaces. His research is focusing the development of advanced nano/microfabrication techniques including lithography, 3D printing, electrospinning, and electrospray, and multi-scale production system based on artificial intelligence. Details can be found https://sites.google.com/view/ipmslab/.